Influences of tectonic and geomorphic processes on fault scarp height along the Teton fault, Wyoming, USA

Grasso, K.

Stantec Consulting Services, Inc., San Bernardino, California, USA Thackray, G.D.

Department of Geosciences – Idaho State University, Pocatello, Idaho, USA



ABSTRACT

Landscape disturbance events (e.g., earthquakes, slope failures) play key roles in landscape evolution in tectonically active areas. Along the Teton fault, fault scarps vary in height by up to tens of meters. LiDAR-based mapping indicates that scarp height is affected by glacial geomorphology, slope failure, and alluvial processes. LiDAR data, digital and field mapping were used to characterize fault scarps and slope failure deposits along the Teton fault zone. Based on vertical separation (VS; the vertical offset between faulted surfaces) across fault scarps and the expected behavior of normal faults, we propose a four-section model of the Teton fault. At a broad scale, VS is greatest along the southern fault zone. At a finer scale, VS is least at the ends of the fault and at three areas within the central fault zone. Transitions between these four sections may represent segment boundaries with potentially important implications for geohazards assessment.

RÉSUMÉ

Les événements de perturbation du paysage (p. ex., tremblements de terre, ruptures de pente) jouent un rôle clé dans l'évolution du paysage dans les zones tectoniques actives. Le long de la faille de Teton, les escarpements de faille varient en élévation jusqu'à des dizaines de mètres. L'interprétation des données lidar indique que la hauteur des escarpements est affectée par la géomorphologie glaciaire, les ruptures des pentes et les processus alluviaux. Les données lidar et la cartographie numérique et de terrain ont été utilisées pour caractériser les escarpements de faille et les dépôts de rupture de pente le long de la zone de faille. Sur la base d'une séparation verticale (VS; différence d'élévation entre les surfaces faillées), des escarpements de faille et du comportement attendu des failles normales, nous proposons un modèle à quatre sections de la faille de Teton. À petite échelle, VS est plus élevée dans la section sud de la faille. À plus grande échelle, VS est plus faible aux extrémités de la faille, ainsi qu'à trois emplacements situés dans la section centrale de la faille. Les transitions entre ces quatre sections représentent des limites ayant des implications potentiellement importantes pour l'évaluation des géorisques.

1.0 INTRODUCTION

The Teton fault is expressed as a 75-km long series of north-northeast trending normal fault scarps on the eastern flank of the Teton Range (Figure 1). We identify and characterize fault scarps and slope failure deposits, patterns of vertical separation (VS) across fault scarps, and discusses the implications of variable scarp height as it pertains to fault segmentation and geohazards assessment along the Teton fault.

Landscape disturbance events (e.g., earthquakes, slope failures) play key roles in landscape evolution in tectonically active areas (Keefer, 1984). Similarly, glacial and alluvial processes alter landscapes and influence sediment flux in alpine environments (McColl and Davies, 2013). Smaller-scale processes (e.g., erosion, hillslope diffusion) also influence landscapes. These processes alter the surface expression of faults, introducing complexity along range fronts.

Teton fault scarps vary in height by up to tens of meters along the fault. Scarps offset glacial and alluvial landforms, providing diachronous and synchronous markers of fault movement (Byrd, 1995; McCalpin, 1996; Thackray and Staley, 2017). Spatial and temporal variations of fault

motion are reflected in paleoseismic trench and geomorphological observations (Byrd, 1995; Thackray and Staley, 2017; Zellman et al., 2018, 2019; DuRoss et al., 2019). Variable scarp height may result from: 1) along-strike, variable fault offset rates; 2) variable erosion of the fault scarp; 3) postglacial erosion and burial by slope failure and alluvial processes; or 4) some combination of these or other factors. The influences of these processes on fault scarp geomorphology, and the influences of fault slip on these processes and their resultant landforms, are the subject of this study.

1.2 Geologic setting

Uplift of the Teton Range began with Laramide Orogeny thrust faulting in Late Cretaceous and early Paleogene time. The Laramide Orogeny uplifted Precambrian, Paleozoic and Mesozoic rocks along the Cache Creek thrust fault, creating the Teton-Gros Ventre uplift (Love et al., 2003). Movement along the Cache Creek thrust at the southern end of the modern Teton Range vertically offset Precambrian rocks exposed in the area by up to 6 km (Smith et al., 1993). As uplift was took place, reverse faults formed across the Teton-Gros Ventre region, increasing displacement (Love et al., 2003). The resultant landscape

was further modified by uplift of the Teton fault (Roberts and Burbank, 1993; Love et al., 2003; Brown et al., 2017).

The core of the Teton Range is broadly composed of metamorphosed intrusive and metasedimentary rocks of the Archean Webb Canyon Gneiss and Proterozoic Mount Owen Quartz Monzonite (Love et al., 1992, 2003). Quaternary deposits are mapped at the surface in many areas (Love et al., 1992; Pierce and Good, 1992; Pierce et al., 2018).

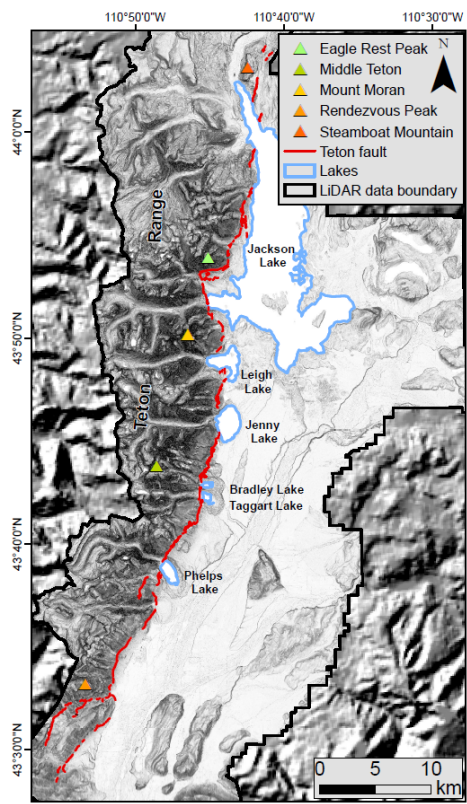


Figure 1. Study area. The study area spans an approximately 1-km wide swath along the Teton fault.

1.3 Glacial history

The Teton region was repeatedly glaciated during Pleistocene time, generating key markers for estimating fault slip rates. Geomorphic evidence of the two most recent glaciations, the Bull Lake (BL) and Pinedale (PD), is widely preserved in the area. During BL and PD glacial time, ice from two sources impacted the Teton Range. The Greater Yellowstone Glacial System (GYGS) flowed into Jackson Hole from the north and northeast, and mountain glaciers flowed easterly down major valleys (Licciardi et al., 2014a, 2015; Pierce et al., 2018).

Moraines and outwash surfaces extending to the southern end of Jackson Hole record the advance of the GYGS from the north (Licciardi and Pierce, 2008, 2018; Pierce et al., 2011).

The retreat of BL-age ice was followed by advance and retreat of GYGS-sourced ice during three phases of the PD glaciation, spanning ~22-13 ka (Love et al., 1992; Pierce

and Good, 1992; Licciardi and Pierce, 2008, 2018). During GYGS advances, Yellowstone ice cap glaciers advanced into Jackson Hole from the east and north, while mountain glaciers descended eastward in the Teton range to intersect with Yellowstone ice in the Jackson Lake area or to flow into the margins of Jackson Hole (Licciardi and Pierce, 2008; Pierce et al., 2018).

Pinedale-age glacial ice retreated from the study area approximately 15 ka. In the study area, PD glacial activity is recorded as a series of lateral and terminal moraines (Licciardi and Pierce, 2008; Pierce et al., 2018), by alluvial landforms, and by deeply eroded valley floors.

2.0 METHODS

2.1 Digital mapping

The study area was digitally mapped using 1-m resolution LiDAR data (Woolpert, Inc., 2015) and ArcGIS version 10.7.1 software. Data was provided to USGS in ERDAS .IMG format with 1 m cell size and vertical error ranging from -0.194 m to 0.135 m with an average of 0.027 m after hydrologic flattening was conducted.

LiDAR-based digital elevation (DEM), hillshade, slope, and topographic models were used to construct a geomorphic map of the study area using methods similar to those of Harding (2000), Burns and Madin (2009), and Crawford (2012). Fault scarps were mapped based on geomorphic characteristics including length, height, cross-sectional shape and slope angle, and cross-cutting relationships with other surficial landforms. Slope failure deposits were mapped following the general guidelines of Burns and Madin (2009).

2.2 Scarp profiling

Topographic profiles across fault scarps were measured using the ArcGIS profiler tool. Profiles were measured perpendicular to the strike and at approximately 1 km intervals along the fault. Profiling sites were selected where landform surfaces on either side of the scarp appear to be synchronous. Profile locations were chosen to capture data across the highest scarps with similar surface slopes on the hanging wall and footwall sides of the fault, reflecting the highest recorded VS while minimizing the effects of erosion and other height-reducing processes. Scarps impacted by slope failures or other erosive events were not profiled.

2.3 Vertical separation and simple scarp height

Simple scarp height (SSH) and VS were calculated at fifty scarp profiling locations along the fault. Here, SSH is the vertical distance between the highest and lowest points across the scarp, while VS is the restored vertical distance between the tectonically undeformed footwall and hanging wall surfaces. Vertical separation was calculated following the methods Thompson et al. (2002) and Amos et al. (2010) and is illustrated in Figure 2.

Linear regression lines were projected along the offset faulted surfaces at each profile location. The slope angle of each surface was calculated from the arctangent of the slope of the best-fit line for each surface (Equation 1). The VS was calculated at the scarp midpoint, following the methods of McCalpin (1996).

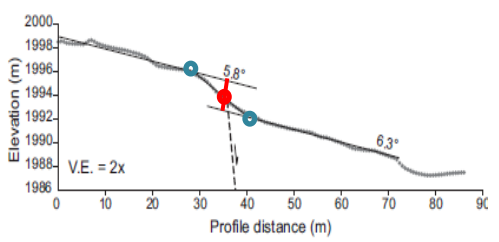


Figure 2. Topographic profile with linear regression lines through the footwall and hanging wall surfaces. Vertical separation (red line) is calculated as the distance between the regression lines (straight black lines, center) at the midpoint along the scarp (red circle). SSH is calculated as the elevation difference between the lowest and highest points (blue circles) on the scarp. Modified from Amos et al. (2010).

Equation 1: Calculation of slope of the best-fit linear regression line for points defining the footwall and hanging wall surfaces:

Slope angle in degrees = arctan(m),

where m is the slope of the linear regression line through the surface being considered.

Profiles with similar slope angles on both the footwall and hanging wall surfaces provide the best estimate of VS across fault scarps by reducing measurement error.

Sturge's rule provides a formula for determining an appropriate number of bins and bin division values for data displayed in histogram format (Scott, 2009). Fault scarp profiles were classified as low-, moderate-, and high-quality based on similarity of the slope angle between the footwall and hanging wall by applying Sturge's Rule (Equation 2). Profiles classified as low quality (n=4) and where calculated VS exceeded SSH (n=4) were eliminated from further analyses.

Equation 2. Sturge's rule:

Number of bins = 1+3.322*log(n)

where n is the number of data points being considered

Hanging wall and footwall slope angle differences were binned into seven classes based on Sturge's Rule. Surface angle contrasts <3.46° were classified as high quality (i.e., lower uncertainty in the VS measurement), those with surface angle contrast between 3.46° and 10.27° were classified as moderate quality, and those with surface angle contrast >10.27° were classified as low quality, interpreted as having higher uncertainty in the VS measurement.

2.4 Field Mapping

Field mapping was conducted in selected areas along the fault in 2019. Mapping confirmed the relationships between scarps, slope failure deposits, and other features which were mapped digitally.

3.0 RESULTS

Slope failure deposits mapped in the study area fall into two categories: translational slides and debris flows. Lateral moraines, moraine crests, and drumlin crests were also mapped based on geomorphic characteristics.

3.1 Fault scarp mapping

The Teton fault is expressed at the surface as a series of scarps that offset glacial and alluvial landforms. Fault scarps show a consistent sense of normal, down-to-the-east displacement along the fault zone. Simple scarp height and VS were measured across forty-two scarp-normal profiles. Simple scarp height ranges from 7 m to 70 m and VS ranges from 1.0 m to 54.4 m across the profiles.

The southern 10 km of the fault zone is characterized by a bifurcation of the main fault into two separate strands, the Phillips Valley fault to the west, and the Teton fault to the east (Figure 1).

3.2 Scarp profile analysis

The average VS across the forty-two high- and mediumquality profiles is 14.5 m, and 15.4 m across all profiles. At a broad scale, VS is greatest along the southern fault. At a finer scale, VS is less at the ends of the fault and at three locations within the central fault zone, and higher between these areas.

3.3 Slope failure deposits

Both large- and small-scale slope failure deposits are evident in the study area. Translational and flow deposits of earth, rock, and debris range in size up to 2.3 km², although most deposits are <0.1 km². Most slope failures occur in PD-age glacial deposits and along deglaciated valley walls, although they are also found on steep slopes of varying orientation and rock type.

3.4 Field mapping results

Field mapping improved the accuracy of final map products by eliminating features for which geomorphic evidence was lacking or led to new interpretations of features. Soil and vegetation along the range front limit surface exposures of bedrock units in much of the study area. Deposits of glacially transported material and alluvium are common and cover much of the area. Rock units exposed at the surface were correlated to those of Love et al. (1992).

4.0 INTERPRETATION AND DISCUSSION

The more detailed dataset of VS presented here indicates that previous fault section interpretations (Susong et al.,

1987; Smith et al., 1993) can be improved by considering the expected behavior of normal faults. We propose a four-section model of the Teton fault based on VS analysis and expected patterns of fault behavior. In this context, a fault section is an area along a fault which is typically identifiable from generalized characteristics, while fault segments represent individual parts of a fault which may rupture independently of one another during an earthquake event. This work indicates that a four-section, or possibly segment, model of the Teton fault should be considered.

4.1 Simple scarp height and vertical separation

Simple scarp height reflects fault offset rates and the surface slope of landforms cut by faulting. Geometric relationships between surface slope and fault offset lead to higher where the slope of pre-existing surfaces is steep. Measurements of VS account for this effect and provide a better understanding of fault offset patterns. Vertical separation across scarps varies along the length of the Teton fault. Individual scarps are vertically separated by up to 54.4 m (average 14.5 m), and the highest scarps are found along the southern range front and Phillips Canyon.

Along-strike variation in SSH and VS may be the result of 1) along-strike, variable offset rates of the Teton fault; 2) variable erosion of fault scarps by Pleistocene glacial processes; 3) variable ages of landforms; 4) erosion and deposition by slope failure and alluvial processes that have occurred since deglaciation; or 5) some combination of these factors, and possibly others.

1) Along-strike variable offset rates

Estimations of offset rate along the strike of the Teton fault suggest that variable scarp height may be the result of variable offset rates along the Teton fault. The offset rate may vary between sections and within sections of the fault. Vertical separation across fault scarps combined with surface exposure ages of deglacial landforms can be used to estimate VS rates. Using the average VS measurement across five scarp profiles and the age of the deglacial surface (14.4±0.8 ka; Licciardi and Pierce, 2018), we calculate a VS rate of 0.32±0.01 m/k.y. for the area northeast of Jackson Lake.

Thackray and Staley (2017) calculated a VS rate of 0.82 ±0.13 m/k.y. over the past 14.7 k.y. from valley floor offsets of well-constrained deglacial age in the central portion of the fault but found these values to be inconsistent with data from higher, and geomorphically older, landforms. Using data from the Buffalo Bowl and Granite Canyon paleoseismic studies, DuRoss et al. (2019) calculate a latest Pleistocene (14.4-4.7 ka) closed-interval vertical slip rate of ~1.1 m/k.y. for the southern Teton fault and an early Holocene to present open-ended rate of ~0.6 m/k.y, indicating that along-strike variable offset rates could contribute to variable scarp height.

2) variable erosion of fault scarps by Pleistocene glacial processes

Glaciers play a key role in shaping mountain valleys through sediment production, transportation, and deposition (Hallet et al., 1996; Foster et al., 2010). These

factors have likely impacted degradation of Teton fault scarps. Because the effects of fault scarp erasure by glacial processes have not been studied in the Teton Range or elsewhere, we assume that glacial erosion and deposition reduced the scarp height to match valley floor topography, effectively erasing the pre-existing scarps within glacial valleys.

Assuming this is the case, deglaciated valleys provide an opportunity to compare VS across landforms of assumed similar age. Pinedale age glacial activity is recorded as a series of glacially eroded valleys (on the footwall), sediment filled valleys (on the hanging wall), and lateral and terminal moraines mantling the range front and the Teton fault (Licciardi and Pierce, 2008; Pierce et al., 2018). At the mouth of Glacier Gulch, the valley floor scarp has vertically separation of ~9.9 m. At Phelps Lake, VSs of ~6.6 m and ~14.0 m are recorded on the valley floor and right lateral moraines, respectively.

3) variable ages of landforms

The ages of range front landforms and lake sediments have been determined from cosmogenic ¹⁰Be surface exposure and radiocarbon dating along the Teton fault (Licciardi and Pierce, 2008; Licciardi et al., 2014a, 2014b, 2015; Larsen et al., 2016; Pierce et al., 2018). Landforms of varying age pose a challenge to addressing fault scarp height variability. Scarps cutting older landforms have likely experienced more slip events than those cutting younger landforms, and thus have higher scarps. Landform age plays a critical role in addressing fault scarp height variation.

At Taggart Lake, VS of ~14.7 m and ~12.5 m across the highest fault scarps on the left and right lateral moraines, respectively, allow for evaluation of VS across varying time scales. The moraine ages are 18.2±0.5 ka and 15.1±0.2 ka, respectively, based on preliminary interpretation of cosmogenic ¹⁰Be surface exposure dating (Licciardi et al., 2019; Licciardi, pers. comm.). Using these values, both the left and right lateral moraines have undergone similar rates of VS (0.81±0.02 m/k.y. and 0.91±0.01 m/k.y., respectively). Variable landform age appears to explain the difference in VS across these moraines.

4) erosion and deposition by slope failure and alluvial processes that have occurred since deglaciation

Slope failure deposits affect the surface expression of scarps along the Teton fault. Individual slope failure-affected areas are up to 2.4 km², but most slope failure deposits cover <0.1 km² in the study area.

Where slope failures initiate above and cross fault scarps, the surface expression of the fault scarp is reduced or obscured by the deposit, effectively reducing the height of scarps in these areas. Few slope failure deposits are cut by scarps of the Teton fault; however, there are notable exceptions to this pattern north of Leigh Lake and south of Phelps Lake, where fault scarps are vertically separated by 42.8 and 14.6 m, respectively.

5) some combination of these factors, and possibly others. Variable fault offset rates, variable erosion by glacial processes, and erosion by slope failure and alluvial

processes, or other factors, may all influence the size of fault scarps individually or in concert. Landscape disturbance events (e.g., earthquakes, slope failures) may be triggered by movement of the Teton fault.

4.2 Fault sections, fault segments, and their boundaries

The number of segments and the location of segment boundaries along the Teton fault have been the subject of debate, as has the identification of fault sections and segments in general (Crone and Machette, 1984; Machette et al., 1991; Smith et al., 1993; Faulds and Varga, 1998; O'Connell et al., 2003; DuRoss et al., 2019). Within the central fault zone, Susong et al. (1987) proposed a three-segment model of the fault based on field mapping and scarp profiles at 17 locations. Smith et al. (1993) proposed a three-segment model of the fault with segments defined by changes in strike direction, lateral stepping, structural complexities, variation in scarp height, and interpretation of gravity data.

The three-segment interpretations are contrasted by gravity anomaly data which suggest the fault as being divided into two segments (Ostenaa, 1988). However, many of the commonly referenced indicators of segmentation are distinctly two-dimensional in nature, and the two-dimensional nature of geologic maps and the limited ability of many study approaches may contribute to misunderstandings of fault growth and segmentation (Walsh et al., 2003).

We propose a four-section model of the Teton fault based on VS across fault scarps and changes in strike direction. From north to south, these are the Eagle Rest Peak (ERP), Mount Moran (MM), Middle Teton (MT), and Rendezvous Peak (RP) sections (Figures 3 and 4). The ERP section extends from northeast of Jackson Lake south to Moran Bay. The MM section extends from north of Moran Bay to the south end of Jenny Lake. The MT section reaches from south Jenny Lake to Granite Canyon. The RP section extends from Granite Canyon to the south end of the fault at Teton Pass. Vertical separation is greatest toward the central portion of each of these sections and declines toward the ends, following the expected pattern of normal fault behavior.

Applying a four-point moving average trendline to the VS data points highlights the finer pattern of height variability (Figure 3). The four-point average highlights broader variability while also representing local anomalies. The trendline suggests that VS increases toward the central portion of four separate areas, with each area separated by several scarps with low VS.

The ERP section is characterized by NNE-striking fault scarps and VS ranging from 1.0 to 21.3 m (average 11.9 m) based on analysis of 18 scarp profiles distributed along 22 km of the fault. We calculate a VS rate of 0.32±0.01 m/k.y. using the average VS across the five scarp profiles cutting drumlinoid topography northeast of Jackson Lake and a surface age of 14.4±0.8 ka (Licciardi and Pierce, 2018).

The MM section is characterized by VS ranging from 1.6 m to 32.0 m (average 15.0 m) based on analysis of 7 scarp profiles distributed along 15 km of the fault. We calculate a VS rate of 0.68±0.03 m/k.y. across the Jenny

Lake right lateral moraine using a surface exposure age of 15.2±0.7 ka from Licciardi and Pierce (2018).

The MT section is characterized by a NNE-striking fault and VS ranging from 6.6 m to 14.8 m (average 12.2 m) based on analysis of from 11 scarp profiles distributed along 16 km of the fault. We calculate a VS rate of 0.91±0.01 m/k.y. across the left lateral moraine at Taggart Lake using a surface exposure age of 15.1±0.2 ka from Licciardi et al., 2019. A VS rate of 0.81±0.02 m/k.y. across the right lateral moraine at Taggart Lake using a surface exposure age of 18.2±0.5 ka from Licciardi et al., 2019.

The RP section is characterized VS ranging from 13.6 to 54.4 m (average 26.1 m). Anomalously high scarps in this section are found in several locations along both the Phillips Valley and Teton fault strands. We calculate a VS rate of 0.70±0.01 m/k.y. across the right lateral moraine at Granite Canyon using a surface exposure age of 18.24±0.34 ka (Licciardi et al., 2014a).

Surface age data are limited in the RP section. Two distinct VS rates have been calculated using the average VS across the five southernmost scarp profiles (25.8 m) and two assumed ages. The first, using the PD surface exposure age from the right lateral moraine at Granite Canyon, provides a VS rate of 1.6±0.02 m/k.y. The second, calculated using a BL surface exposure age of 136±0.34 ka from boulders in Jackson Hole (Licciardi and Pierce, 2008), provides a VS rate of 0.21±0.03 m/k.y.

If scarps along the southern range cut PD-age deposits, the VS rate along the southern fault is higher than other more well-constrained VS rates calculated along the fault. However, if these scarps cut surface deposits of BL-age, the VS rate along the southern range front is less than the VS rate for scarps cutting PD-age deposits to the north. It is also possible that the fault cuts landforms of both ages and that these rates, based on average VS, are not meaningful.

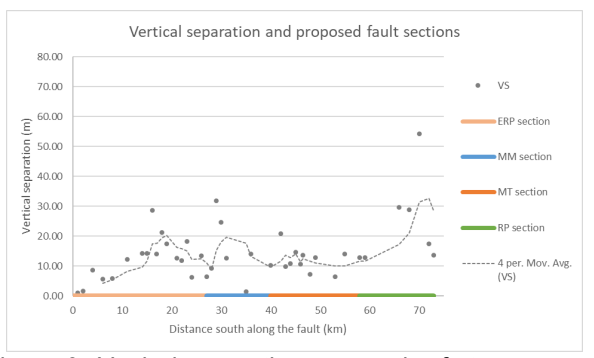


Figure 3. Vertical separation across the forty-two scarp profiles and the extent of the four proposed fault sections. Dashed line is a four-point moving average trendline highlighting the overall pattern of VS along the fault. Proposed section names based on local landmarks as follows: ERP – Eagle Rest Peak; MM – Mount Moran; MT – Middle Teton; RP- Rendezvous Peak (see Figure 4).

The transition zones between these four distinct areas may represent boundaries between fault sections or segments. The sections proposed here are based on data that represent the behavior of the fault in Middle to Late Pleistocene time. Data from paleoseismic trenching

studies indicate that the most recent surface rupturing event on the Teton fault took place 4-5 ka; this may indicate that sections (or segments) of the fault rupture in unison, or have done so recently (Zellman et al., 2019; DuRoss et al., 2019). However, further paleoseismic work is needed to clarify the rupture history and potential for segmentation along the fault.

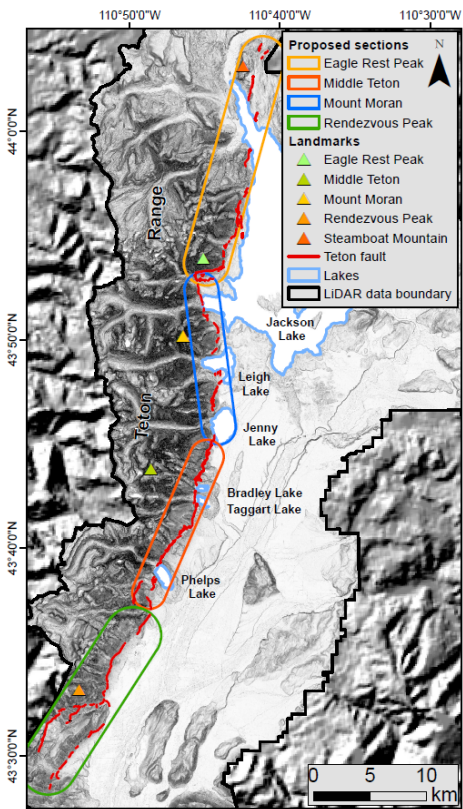


Figure 4. The proposed four-section model of the Teton fault based on VS analysis.

Uncertainty in these approaches comes from four primary sources: 1) fault scarps cut complex landforms, leading to uncertainty when choosing the top and bottom points of the scarp used for calculating SSH and VS; 2) geomorphology is complex and surface age data are limited; 3) the ArcGIS profiler tool extracts data from the LiDAR-based DEM at a set resolution, introducing a small level of error in profile measurement; and 4) higher fault scarps increase the uncertainty of both SSH and VS calculations (Thackray and Staley, 2017)

4.3 Surface expression of the fault varies across five geomorphic areas

Surface expression of fault scarps varies along the length of the Teton fault. Five geomorphic areas with unique surface expression of the fault have been identified in the study area: 1) drumlins in PD-age ice cap outlet lobe deposits northeast of Jackson Lake; 2) scarps cutting glacial outwash and alluvial fans between Jackson and Jenny Lakes; 3) PD-age lateral moraines; 4) PD-age deglaciated valley floors; and 5) the southern range front,

where the age of surface deposits remains largely unknown.

4.4 Slope failures tend to be larger in the northern half of the study area and smaller in the southern half of the study area.

Slope failure deposits in the study area are interpreted as translational slide and debris flow deposits. North of Leigh Lake, translational slide deposits are more common than debris flow deposits. Slide deposits tend to be larger in this area than those found in the southern half of the study area, covering up to 2.4 km². South of Leigh Lake, translational slide deposits up to 2.3 km² were mapped, but most deposits are <0.5 km². Most debris flow deposits are found within the southern half of the study area (Figure 5).

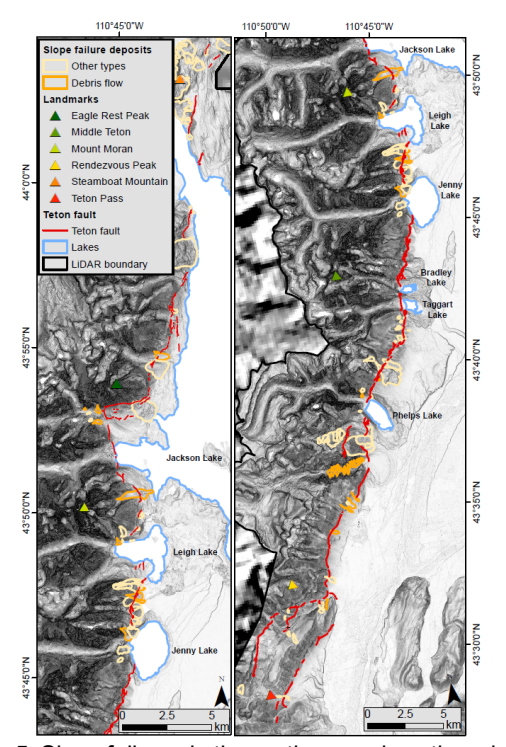


Figure 5. Slope failures in the northern and southern halves of the study area.

5.0 CONCLUSIONS

Teton fault scarps vary in height by up to tens of meters over short (<1 km) and longer distances. LiDAR data reveal these scarps and provide an opportunity to use VS across fault scarps to address questions of fault section or segment boundaries. Scarp height has been influenced by glacial, hillslope, and alluvial processes, as well as apparent slip rate variations, resulting in variable fault scarp height along the length of the Teton fault.

Variable scarp height indicates a four-section model of the Teton fault should be considered. Previously proposed models of the Teton fault suggest that it is composed of two to three segments (Ostenaa, 1988; Smith et al., 1993). The greatest slip rate is expected to be concentrated within the central portions of normal faults, resulting in a systematic increase in VS toward the central portion of the fault (Cowie and Roberts, 2001).

Vertical separation across scarp profiles indicates that the fault does not follow the expected pattern of normal fault behavior. However, the pattern is observed within four discrete sections of the fault. Based on VS analysis, we propose a four-section model of the Teton fault with section boundaries at Moran Bay, south Jenny Lake, and Granite Canyon. Each of these sections are characterized by a pattern of VS across fault scarps which increases toward the central portion of the area. The transition zones between these four areas may represent boundaries between fault sections or segments.

Scarps at the southern end of the fault are high. South of Granite Canyon, fault scarps with anomalously large (>15 m) VS are common. Anomalously high scarps may reflect greater landform age, variable fault slip rate, or a combination of these factors. Dating of these landforms would clarify the VS rates in this southern area and their relationship to the rest of the fault system.

Slope failures tend to be larger in the northern half of the study area and smaller in the southern half of the study area. Translational slope failure deposits are more common along the northern Teton fault, while debris flow deposits are more common along in the southern range. Along deglaciated valley walls, south-facing slopes are more prone to debris flow activity than north-facing slopes.

6.0 REFERENCES

- Amos, C.B., Kelson, K.I., Rood, D.H., Simpson, D.T., and Rose, R.S. 2010. Late Quaternary slip rate on the Kern Canyon fault at Soda Spring, Tulare County, California: *Lithosphere*. 2: 411–417.
- Brown, S.J., Thigpen, J.R., Spotila, J.A., Krugh, W.C., Tranel, L.M., and Orme, D.A. 2017. Onset Timing and Slip History of the Teton Fault, Wyoming: A Multidisciplinary Re-evaluation: *Tectonics*, 36: 2669–2692.
- Burns, W.J., and Madin, I.P. 2009. Protocol for Inventory Mapping of Landslide Deposits from Light Detection and Ranging (lidar) Imagery: Oregon Department of Geology and Mineral Industries Special Paper 42: 1-36.
- Byrd, J.O.D. 1995. Neotectonics of the Teton fault, Wyoming [Dissertation]: University of Utah, 1-215.
- Crawford, M.M., 2012, Using LiDAR to Map Landslides in Kenton and Campbell Counties, Kentucky: *Kentucky Geological Survey Report of Investigations*: 1–12.
- Crone, A.J., and Machette, M.N. 1984. Surface faulting accompanying the Borah Peak earthquake and segmentation of the Lost River fault, central Idaho: *Geology*, 12: 664–667.
- Cowie, P.A., and Roberts, G.P. 2001. Constraining slip rates and spacings for active normal faults: *Journal of Structural Geology*, 23: 1901–1915.
- DuRoss, C.B., Gold, R.D., Briggs, R.W., Delano, J., Ostenaa, D., Zellman, M., Cholewinski, N., Wittke, S., and Mahan, S. 2019. Paleoseismic history and

- slip rate of the Teton fault at the Buffalo Bowl site: Seismological Society of America Annual Meeting, Albuquerque, New Mexico, USA.
- Faulds, J.E., and Varga, R.J. 1998. The role of accommodation zones and transfer zones in the regional segmentation of extended terranes, in Accommodation Zones and Transfer Zones: The Regional Segmentation of the Basin and Range Province: Geological Society of America Special Paper 323.
- Foster, D., Brocklehurst, S.H., and Gawthorpe, R.L. 2010. Glacial-topographic interactions in the Teton Range, Wyoming: *Journal of Geophysical Research*, 115: F01007.
- Hallet, B., Hunter, L., and Bogen, J. 1996. Rates of erosion and sediment evacuation by glaciers: A review of field data and their implications: Global and Planetary Change, 12: 213–235.
- Harding, D.J. 2002. Fault scarp detection beneath dense vegetation cover: airborne LiDAR mapping of the Seattle fault zone, Bainbridge Island, Washington State, Proceedings of the American Society of Photogrammetry and Remote Sensing Annual Conference, Washington, D.C., USA, 11.
- Keefer, D.K. 1984. Landslides caused by earthquakes, Geological Society of America Bulletin, 95: 406– 421.
- Love, J.D., Reed, J.C., and Christiansen, A.C. 1992. Geologic Map of Grand Teton National Park, Teton County, Wyoming: United States Geological Survey, 1.
- Love, D.J., Reed, J.C., Jr., and Pierce, K.L. 2003. Creation of the Teton landscape: Moose, WY, Grand Teton History Association in cooperation with the National Park Service: 1-132.
- Lageson, D.L. 1992. Possible Laramide influence on the Teton normal fault, western Wyoming.pdf, in Regional Geology of Eastern Idaho and Western Wyoming, Geological Society of America, Memoir, 179: 121-155.
- Larsen, D.J., Finkenbinder, M.S., Abbott, M.B., and Ofstun, A.R. 2016. Deglaciation and postglacial environmental changes in the Teton Mountain Range recorded at Jenny Lake, Grand Teton National Park, WY: Quaternary Science Reviews, 138: 62–75.
- Licciardi, J.M., and Pierce, K.L. 2008. Cosmogenic exposure-age chronologies of Pinedale and Bull Lake glaciations in greater Yellowstone and the Teton Range, USA: *Quaternary Science Reviews*, 27: 814–831.
- Licciardi, J.M., Pierce, K.L., Finkel, R.C., and Zimmerman, S.H. 2014a. Timing of late Pleistocene glacier culminations and retreat in Grand Teton National Park: *Geological Society of America 2014 Annual Meeting Abstracts with Programs*, 46 (6).
- Licciardi, J., Pierce, K.L., Finkel, R.C., and Zimmerman, S.H. 2014b. Expanded chronology of Late Pleistocene glacial events in the greater Yellowstone and Grand Teton regions: Geological Society of America, v. Rocky Mountain (66th

- Annual) and Cordilleran (110th Annual) Joint Meeting.
- Licciardi, J.M., Pierce, K.L., Thackray, G.D., Finkel, R.C., and Zimmerman, S.R.H. 2015. Cosmogenic 10Be Chronologies of Moraines and Glacially Scoured Bedrock in the Teton Range, with Implications for Paleoclimatic Events and Tectonic Activity: AGU Fall Meeting Abstracts, 51: PP51E-02.
- Licciardi, J.M., and Pierce, K.L. 2018. History and dynamics of the Greater Yellowstone Glacial System during the last two glaciations: Quaternary Science Reviews, 200: 1-33.
- Licciardi, J., Pierce, K., Thackray, G., Zellman, M., Larsen, D., and Schweinsberg, A. 2019. Late Pleistocene glacier chronologies and fault slip rates in the Teton Range, USA, revealed by 10Be dating of fault-displaced moraines: *International Union for Quaternary Research*, Dublin, Ireland.
- Machette, M.N., Personius, S.F., Nelson, A.R., Schwartz, D.P., and Lund, W.R. 1991. The Wasatch fault zone, Utah—segmentation and history of Holocene earthquakes: *Journal of Structural Geology*, 13: 137–149.
- McCalpin, J.P. 1996. *Paleoseismology*: San Diego, California, Academic Press: 1-588.
- McColl, S.T., and Davies, T.R.H. 2013. Large icecontact slope movements: Glacial buttressing, deformation and erosion: *Earth Surface Processes and Landforms*, 38: 1102–1115.
- O'Connell, D.R.H., Wood, C.K., Ostenaa, D.A., Block, L.V., and LaForge, R.C. 2003. Ground Motion Evaluation for Jackson Lake Dam, Seismotectonic and Geophysics Group, Technical Service Center, Bureau of Reclamation Final Report 2003–2: 1-493.
- Ostenaa, D.A. 1988. Late Quaternary behavior of the Teton fault, Wyoming: *Geological Society of America Abstracts with Programs*, 20: A14.
- Pierce, K.L., and Good, J.D. 1992. Field Guide to the Quaternary Geology of Jackson Hole, Wyoming: *United States Geological Survey Open-File Report* 92–504: 1-59.
- Pierce, K.L., Muhs, D.R., Fosberg, M.A., Mahan, S.A., Rosenbaum, J.G., Licciardi, J.M., and Pavich, M.J. 2011. A loess-paleosol record of climate and glacial history over the past two glacial-interglacial cycles (~150ka), southern Jackson Hole, Wyoming: *Quaternary Research*, 76: 119–141.
- Pierce, K.L., Licciardi, J.M., Good, J.M., and Jaworowski, C. 2018. Pleistocene Glaciation of the Jackson Hole Area, Wyoming: U.S. Geological Survey Professional Paper 1835: U.S. Geological Survey Professional Paper 1835: 1-68.
- Scott, D.W. 2009. Sturges' rule: Wiley Interdisciplinary Reviews: *Computational Statistics*, 1: 303–306.
- Smith, R.B., Byrd, J.O.D., and Susong, D.D. 1993. The Teton Fault, Wyoming: Seismotectonics, Quaternary history, and earthquake hazards: Geological Survey of Wyoming Memoir, 5: 628–667.

- Susong, D.L., Smith, R.B., and Bruhn, R.L. 1987. Earthquake Hazards of the Grand Teton National Park Emphasizing the Teton Fault: *University of Wyoming-National Park Service Research Station Annual Reports*, 11: 106-130.
- Thackray, G.D., Rodgers, D.W., and Streutker, D. 2013. Holocene scarp on the Sawtooth fault, central Idaho, USA, documented through lidar topographic analysis: Geology, 41: 639–642.
- Thackray, G.D., and Staley, A.E. 2017. Systematic variation of Late Pleistocene fault scarp height in the Teton Range, Wyoming, USA: Variable fault slip rates or variable landform ages? *Geosphere*, 13: 287–300.
- Thompson, S.C., Weldon, R.J., Rubin, C.M., Abdrakhmatov, K., Molnar, P., and Berger, G.W. 2002. Late Quaternary slip rates across the central Tien Shan, Kyrgyzstan, central Asia: Slip Rates Across the Kyrzgyn Tien Shan, *Journal of Geophysical Research: Solid Earth, 107: ETG 7-1-ETG 7-32.*
- Pierce, K.L., and Good, J.D. 1992. Field Guide to the Quaternary Geology of Jackson Hole, Wyoming: *United States Geological Survey Open-File Report* 92–504, 1-59.
- Pierce, K.L., Licciardi, J.M., Good, J.M., and Jaworowski, C. 2018. Pleistocene Glaciation of the Jackson Hole Area, Wyoming: *U.S. Geological* Survey Professional Paper 1835: 1-68.
- Pierce, K.L., Muhs, D.R., Fosberg, M.A., Mahan, S.A., Rosenbaum, J.G., Licciardi, J.M., and Pavich, M.J. 2011. A loess-paleosol record of climate and glacial history over the past two glacial-interglacial cycles (~150ka), southern Jackson Hole, Wyoming: *Quaternary Research*, 76: 119–141.
- Roberts, S.V., and Burbank, D.W. 1993. Uplift and thermal history of the Teton Range defined by apatite fission-track dating: *Earth and Planetary Science Letters*, 118: 295–309.
- Scott, D.W. 2009. Sturges' rule: Wiley Interdisciplinary Reviews: *Computational Statistics*, 1: 303–306.
- Walsh, J.J., Bailey, W.R., Childs, C., Nicol, A., and Bonson, C.G. 2003. Formation of segmented normal faults: a 3-D perspective: *Journal of Structural Geology*, 25: 1251–1262.
- Woolpert, Inc. 2015. Grand Teton and National Elk Refuge Airborne LiDAR Task Order Report: *LiDAR data Report*, 1-48.
- Zellman, M.S., DuRoss, C.B., Thackray, G.D., Briggs, R.W., Cholewinski, N., Reyes, T., Patton, N., and Mahan, S.A. 2018. A Paleoseismic Investigation of the Northern Teton Fault at the Steamboat Mountain Trench Site, Grand Teton National Park, Wyoming: Seismological Society of American Annual Meeting, Miami, Florida, USA.
- Zellman, M.S., DuRoss, C.B., and Thackray, G.D. 2019. The Teton Fault, Teton County, Wyoming: Wyoming Geological Survey Open File Report 2019-1: 1.